Dalton Transactions

ROYAL SOCIETY OF CHEMISTRY

PAPER

View Article Online
View Journal | View Issue

Cite this: *Dalton Trans.*, 2022, **51**, 6944

Growth, structure, and temperature dependent emission processes in emerging metal hexachloride scintillators Cs_2HfCl_6 and Cs_2ZrCl_6

V. Mykhaylyk, *[a] S. S. Nagorny, [b,c] V. V. Nahorna,[b,d] P. Wang, [b,d] M. D. Frogley, [a] L. Swiderski,[e] V. Kolomiets[f] and L. Vasylechko [g]

Crystals of metal hexachlorides Cs_2MCl_6 (M = Hf or Zr) have recently emerged as promising materials for scintillation applications due to their excellent energy resolution. In this work, we investigated the crystal structure and scintillation properties of Cs_2HfCl_6 and Cs_2ZrCl_6 crystals in the broad temperature range from 9 to 300 K. X-ray diffraction data confirmed the same cubic structure (space group *Fm3m*) for Cs_2HfCl_6 and Cs_2ZrCl_6 over the entire examined temperature range. The room temperature scintillation light yield of Cs_2HfCl_6 excited with a ^{137}Cs γ-source is measured to be 24 800 photons per MeV, while Cs_2ZrCl_6 exhibits 33 900 photons per MeV resulting in energy resolutions of 5.3% and 4.5%, respectively. The alpha-to-beta ratio determined at room temperature for 5.5 MeV α-particles from an ^{241}Am source is equal to 0.39 for Cs_2HfCl_6 and 0.35 for Cs_2ZrCl_6. The measurements of scintillation decay curves revealed complex kinetics due to delayed recombination processes. A tangible enhancement of the scintillation yield with heating is observed in the 125–150 K range. This effect is a manifestation of negative thermal quenching explained by thermal activation of trapped carriers. A model of the emission centre is proposed that consistently explains the observed changes of emission intensity with temperature in the crystals under study.

Received 23rd January 2022,
Accepted 22nd March 2022

DOI: 10.1039/d2dt00223j

rsc.li/dalton

1. Introduction

The scintillation method of detecting ionizing radiation and particles is broadly used in scientific research, nuclear security and medical diagnostics. The key component of any scintillation detector is the scintillating compound, whose properties often determine the performances of the detection technique. New scintillation materials with improved performance characteristics (such as a high light yield and superior energy resolution) are always sought after and, hence, their development is a vibrant area of scientific research. The materials that belong to the halide family remain the focus of attention and over the last decade many complex halide compounds with promising characteristics have been discovered (see *e.g.* ref. 1 and reference therein). However, only a few materials showed potential for further development and commercialisation due to several reasons, *i.e.* difficulties in synthesis, hygroscopicity, poor consistency of performance and high production cost. It remains a challenge to find materials where these issues can be either avoided or alleviated.

Self-activated metal hexachloride scintillators[2,3] with a general formula Cs_2MCl_6 (M = Hf or Zr), are receiving a great deal of attention. The crystals have a simple structure and exhibit low hygroscopicity – two important properties that compare favourably with other halide scintillators. The first study of Cs_2HfCl_6 carried out by Burger *et al.*[2] quoted an impressive light yield of 54 000 photons per MeV and 3.3% (FWHM) energy resolution for 662 keV γ-rays of ^{137}Cs. The measurements of light yield with energy also revealed that this material has much better non-proportionality of scintillation response in comparison with other halide scintillators. Another important feature of Cs_2MCl_6 scintillators is a low intrinsic radioactivity[4] making these compounds highly desirable for the experimental search of rare nuclear processes occurring in Hf and Zr.[5]

These findings triggered a significant interest in the scientific community and prompted research activity to improve the

[a]*Diamond Light Source, Harwell Campus, Didcot, OX11 0DE, UK. E-mail: vitaliy.mykhaylyk@diamond.ac.uk*
[b]*Arthur B. McDonald Canadian Astroparticle Physics Research Institute, Queen's University Kingston, ON, K7L 3N6, Canada*
[c]*Departments of Physics, Engineering Physics and Astronomy, Queen's University Kingston, ON, K7L 3N6, Canada*
[d]*Chemistry Department, Queen's University Kingston, ON, K7L 3N6, Canada*
[e]*National Centre for Nuclear Research, Soltana 7, 05-400 Otwock, Poland*
[f]*Physics Department I. Franko National University of Lviv, 50 Dragomanova Str., 79005 Lviv, Ukraine*
[g]*Lviv Polytechnic National University, 12 Bandera Str., Lviv 79013, Ukraine*

scintillation characteristics of Cs_2MCl_6 crystals.[6–8] These efforts have been accompanied by extensive theoretical and experimental investigations of the scintillation mechanism which is attributed to the emission of self-trapped excitons (STE).[9–12] In these studies a special attention was paid to the effect of impurities and defects,[13–17] as well as cation and anion substitution[7,18–21] on the scintillation properties. Such a holistic approach enabled targeted optimisation of the manufacturing process that led to the production of large, high-quality scintillation crystals with the enhanced performance characteristics.[22,23]

Despite a significant number of recent studies on scintillation and luminescence properties of Cs_2MCl_6, the information on some physical characteristics of the crystals is incomplete and fragmented. To begin with, there is a lack of accurate crystallographic information for these compounds. The data on the crystal structure of Cs_2HfCl_6 and Cs_2ZrCl_6 published more than 40 years ago[24,25] reveal discrepancies of lattice parameters that hinder the identification of structures. Furthermore, no investigations on temperature changes of the crystal lattice have been published so far. This knowledge is essential to achieve a comprehensive insight into physical properties of the solids and especially for interpretation of their temperature dependence. Lastly, the scintillation properties of Cs_2ZrCl_6 have not been studied to the same extent as these of Cs_2HfCl_6. Lack of such information motivated us to carry out systematic investigations of the crystal structure and scintillation properties of Cs_2HfCl_6 and Cs_2ZrCl_6 crystals in a broad temperature range from 9 to 300 K.

2. Materials and methods

2.1. Preparation of starting materials

Anhydrous CsCl (99.9%), $HfCl_4$ (98%) and $ZrCl_4$ (99.9%) powders were used as starting materials. Due to low initial purity of the $HfCl_4$ and $ZrCl_4$ powders they were subjected to a two-stage sublimation process prior to the synthesis. At the first stage, 50 g of raw $HfCl_4$ or $ZrCl_4$ powder was loaded into a quartz ampoules and sealed under vacuum. Then the sealed tube was placed into a horizontal furnace for sublimation at 400 °C for $HfCl_4$ and 380 °C for $ZrCl_4$. After this stage, the yellow-white $HfCl_4$ or $ZrCl_4$ powders were separated from impurities of dark grey colour. At the second stage of purification, both $HfCl_4$ and $ZrCl_4$ powders were reloaded into new quartz ampules and were then subjected to sublimation at a temperature of 300 °C. The final yields of the two stage purifications were 89% (44.3 g) and 90% (45 g) for $HfCl_4$ and $ZrCl_4$, respectively.

As-received CsCl grains and purified $HfCl_4$ or $ZrCl_4$ powders were mixed in a stoichiometric ratio, thoroughly ground using a mortar and pestle, and then loaded into a tapered quartz ampoule with an inner diameter of 22 mm. Then mixture was dried by heating at 120 °C for 1 hour under vacuum. This was followed by the reduction stage at 300 °C for 1 hour under the flow of hydrogen. The reduced materials were then sealed in the tapered quartz ampoule under a vacuum of 5×10^{-4} mbar.

2.2. Crystal production

Cs_2HfCl_6 and Cs_2ZrCl_6 single crystals were grown by the vertical Bridgman technique. Sealed ampoules with prepared reagents were placed in a furnace and gradually heated to 850 °C. The ampoules were maintained at 850 °C for at least 20 hours prior to the crystal growth to form the Cs_2HfCl_6 or Cs_2ZrCl_6 stoichiometric compounds and to ensure melt homogeneity. Then, the first crystal growth was performed at a pulling rate of 2.7 mm per hour with a temperature gradient of 24 °C cm^{-1} at the solid–liquid interface in the case of Cs_2HfCl_6. In the case of Cs_2ZrCl_6 the pulling rate was 1.5 mm per hour with the temperature gradient of 28 °C cm^{-1}. The obtained boules after this first fast growth were processed to remove all visual impurities or inclusions along with the first-to-freeze sections. The selected crystal pieces were loaded into a new quartz ampoule for the second growth. The second slow crystal growth was performed with pulling rate of 0.7 mm per hour with temperature gradient 42 °C cm^{-1} for the Cs_2HfCl_6 compound, and at the pulling rate of 0.5 mm per hour with temperature gradient 25 °C cm^{-1} for Cs_2ZrCl_6 crystal, correspondingly.

Cs_2HfCl_6 and Cs_2ZrCl_6 crystals of 21 mm diameter and around 60 mm length were obtained (see Fig. 1). The crystal samples with dimensions $7 \times 7 \times 2$ mm for the measurements of optical properties were cut from the tip of the boules by diamond wire saw, and then polished with 1200 grit sandpaper and mineral oil as a lubricant.

2.3. X-ray diffraction studies

The powder samples for X-ray diffraction studies were prepared by grinding the pieces of the crystals in an agate mortar. The sample was then mounted on an Oxford Cryosystems Phenix cold stage allowing measurements at 12–300 K under vacuum. The measurements were performed in a Rigaku SmartLab diffractometer with 9 kW rotating Cu-anode. The data were collected in angular range 10–90° with step 0.01° using a HyPix 3000 2D semiconductor detector. The structural parameters of the crystals were derived from full profile Rietveld refinement of the experimental XRD data using the WinCSD software package.[26] Unit cell dimensions, positional and displacement parameters of atoms were refined together with profile parameters, the texture coefficient in the [111] axis and corrections for absorption and instrumental sample shift.

2.4. Measurements of scintillation properties

For the measurement of pulse height spectra, polished cylindrical crystals of Cs_2HfCl_6 and Cs_2ZrCl_6 with dimensions 20 mm diameter × 12 mm were wrapped in Teflon tape and attached to the window of the photomultiplier tube (R6231-100 PMT, Hamamatsu Photonic, Japan) using an optical grease. The anode signal was sent to a Canberra 2005 preamplifier and then to an Ortec 672 shaping amplifier. The pulse height spectra were collected with 10 μs shaping time, uni-

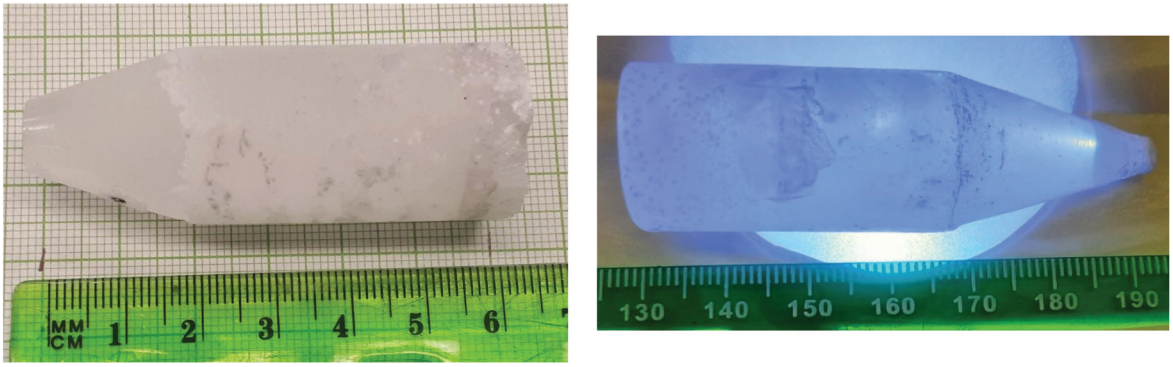

Fig. 1 Left panel: Cs_2HfCl_6 single crystal (daylight illumination). Right panel: Cs_2ZrCl_6 single crystalline boule (illumination by UV lamp). Both crystals have diameter 21 mm and 60 mm in length, with mass of about 60 g each.

polar output. The light yield is obtained by comparing the peak position of the photopeak with that of the single-electron spectrum. The spectra were acquired using a ^{137}Cs source emitting 662 keV γ-rays. An additional ^{241}Am source emitting 5.5 MeV α-particles was used for measurements of alpha-to-beta ratio.

To study scintillation properties with temperature, 7 × 7 × 2 mm polished samples of the crystals were placed in a helium cryostat and excited by 5.5 MeV α-particles from an ^{241}Am source. The scintillation pulses were detected by a multi-alkali photomultiplier tube (PMT) model 9124A (Electron Tube Enterprises, UK). A fast ADC with 10 ns sampling interval was used to digitize the signal from the PMT. This allows resolving individual photons and recording single photon signals. To capture the slow decay component that makes a tangible contribution to the scintillation pulse at low temperature, the signal was recorded over 700 μs. The set of recorded scintillation events (*ca.* 2000) was then analysed off-line. The customised analysis software calculates two histograms: pulse height distribution and distribution of photon arrival times. The first is the measure of a scintillation light yield while the second represents a scintillation decay curve.[27] The measurements were carried out while cooling the crystal to avoid contribution from thermally released charge carriers to the scintillation event observed during heating.

3. Results and discussion

3.1 Crystal structure characterisation with temperature

Fig. 2 shows XRD patterns of the samples measured *in situ* in the temperature range 12–300 K. Analysis of the XRD data revealed that, in addition to the main Cs_2HfCl_6 and Cs_2ZrCl_6 phases, both measured samples contain the admixture phase of CsCl. The appearance of this phase in Cs_2HfCl_6 has previously been explained by incomplete reaction between starting materials due to the high vapor pressure of $HfCl_4$.[20]

Inspection of the XRD patterns for the Cs_2HfCl_6 sample reveals the abnormal relative intensity of several Bragg's maxima, especially pronounced for the [111] direction, indicating strong preferred particle orientations (texture) in the analyzed powder sample. This effect is often observed for powder samples prepared by grinding a bulk single crystal. A similar, though less pronounced, texture effect was also observed in the Cs_2ZrCl_6 sample.

Cooling the samples down to 12 K does not affect the crystal structure and phase composition of the materials. Besides the gradual shift of the Bragg's peak positions due to the lattice contraction, no other visible changes like a reflection splitting and/or appearance of additional peaks were observed in the XRD patterns of Cs_2HfCl_6 and Cs_2ZrCl_6 collected at different temperatures (Fig. 2).

Structural parameters of the Cs_2HfCl_6 and Cs_2ZrCl_6 phases at different temperatures were derived from the corresponding experimental XRD data by a full profile Rietveld refinement. In this procedure, the lattice parameters, atom coordinates and displacement parameters B_{iso} in the main Cs_2HfCl_6 and Cs_2ZrCl_6 structures (space group *Fm*3*m*) were refined together with the profile parameters, the texture coefficient for [111] axis and corrections for absorption and the instrumental sample shift. For the minor CsCl phase only lattice parameters were refined. As a starting model for the Rietveld refinement we adopted the atomic positions of the Cs_2HfCl_6 structure from ref. 24. The refinement procedure led to a good fit between experimental and calculated profiles in all cases. Examples of the Rietveld refinement for Cs_2HfCl_6 and Cs_2ZrCl_6 structures at the selected temperatures are shown in Fig. 3. Obtained structural parameters for Cs_2HfCl_6 and Cs_2ZrCl_6 at 300 and 12 K are summarized in Tables 1 and 2.

The crystal structure of Cs_2MCl_6 (M = Hf, Zr) can be viewed as a variant of the ideal perovskite with the nominal composition ABX_3, where half of the B sites are vacant and the BX_6-octahedra are isolated from one another. Caesium atoms are coordinated by twelve Cl atoms and fill the voids between the MCl_6 octahedra[28] as shown in Fig. 4. These features of the crystal structure recently inspired the dedicated term – vacancy-ordered double perovskites.[29]

Room temperature lattice parameters of Cs_2HfCl_6 and Cs_2ZrCl_6 obtained in this work are in good agreement with the

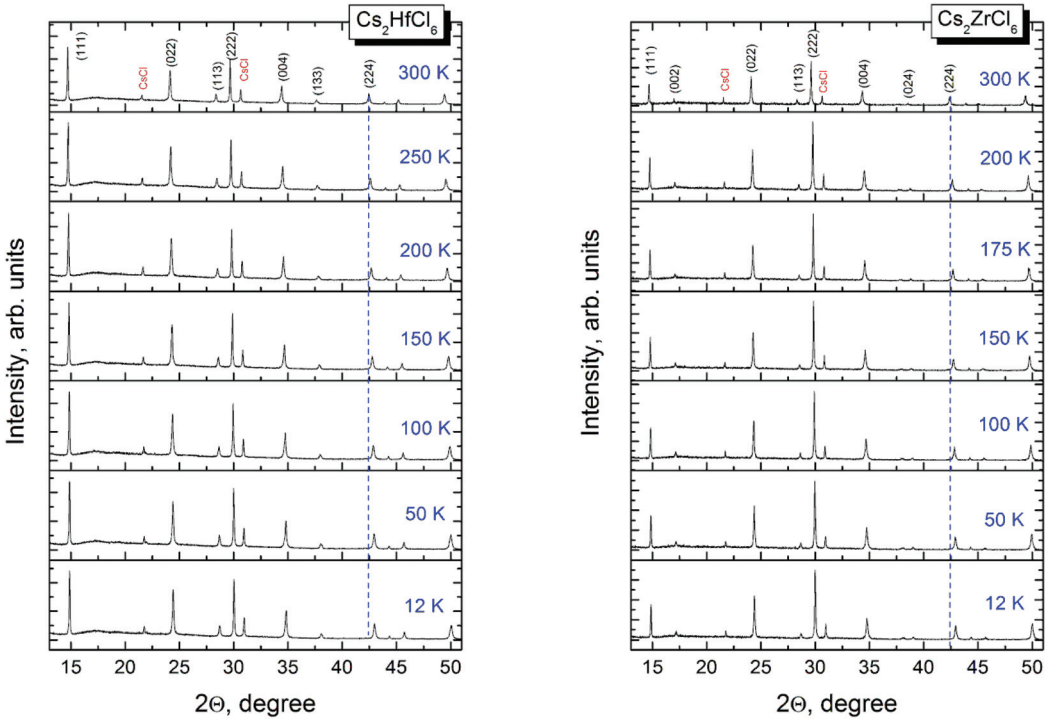

Fig. 2 Evolution of XRD patterns of Cs_2HfCl_6 and Cs_2ZrCl_6 on cooling from 300 K to 12 K. Miller's indices for the corresponding *Fm*3*m* cubic structures and peaks from the CsCl parasitic phase are labelled in the top panels. Vertical dashed lines serve as guide for tracking the shift of Bragg's maxima.

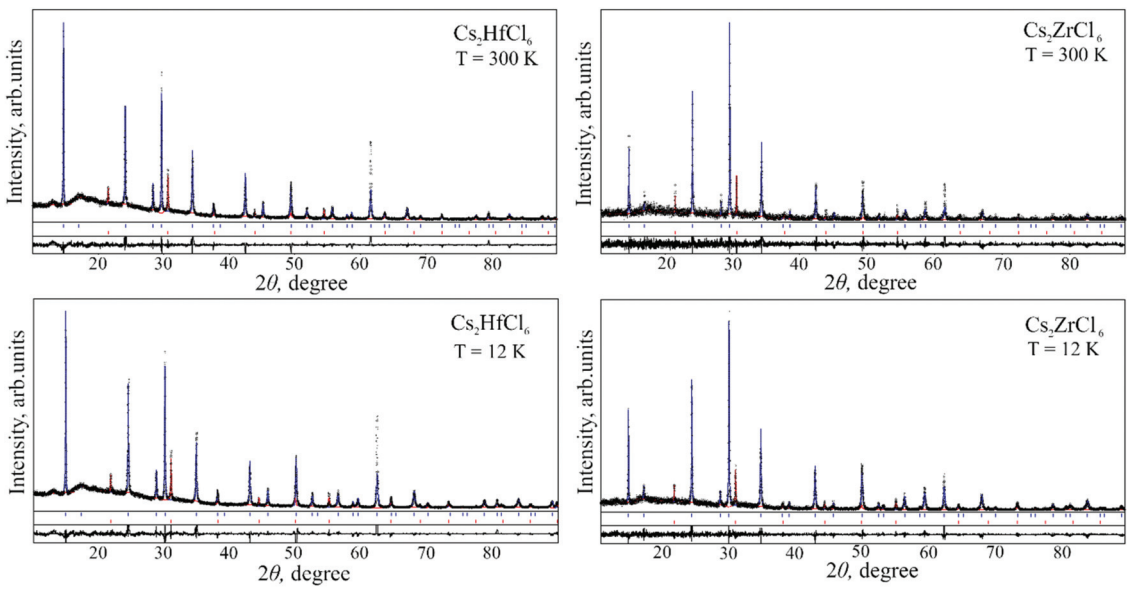

Fig. 3 Graphical results of the Rietveld refinement of Cs_2HfCl_6 and Cs_2ZrCl_6 samples at 300 K and 12 K. Experimental XRD patterns (black dots) are shown in comparison with calculated patterns for the main Cs_2MCl_6 (blue) and admixture CsCl (red) phases. Short vertical bars below the diagrams indicate the positions of Bragg's maxima in corresponding structures.

structural data for these compounds published in ref. 24 and 30, respectively (see Fig. 5). In contrast, the unit cell dimensions of these compounds reported in ref. 25 look rather underestimated. In ref. 31 the lattice parameter of Cs_2ZrCl_6 was predicted based on an empirical model describing the unit cell dimension of cubic A_2MX_6 crystals as a linear function of the ionic radii and electronegativity of the constituting ions.

Table 1 Structural parameters of Cs_2HfCl_6 at 12 K and 300 K (space group *Fm3m*)

Lattice parameter, Å	Atoms, sites	*x*	*y*	*z*	B_{iso}, Å^2
	T = 12 K (R_I = 0.152, R_P = 0.254)				
10.2990(3)	Hf, 4*a*	0	0	0	0.29(8)
	Cs, 8*c*	1/4	1/4	1/4	0.93(8)
	Cl, 24*e*	0.2502(7)	0	0	1.63(15)
Texture axis and parameter: [111] 0.055(1)					
	T = 300 K (R_I = 0.103, R_P = 0.266)				
10.4208(3)	Hf, 4*a*	0	0	0	0.51(9)
	Cs, 8*c*	1/4	1/4	1/4	2.18(11)
	Cl, 24*e*	0.2499(6)	0	0	1.63(15)
Texture axis and parameter: [111] 0.060(1)					

Table 2 Structural parameters of Cs_2ZrCl_6 at 12 K and 300 K (space group *Fm3m*)

Lattice parameter, Å	Atoms, sites	*x*	*y*	*z*	B_{iso}, Å^2
	T = 12 K (R_I = 0.066, R_P = 0.248)				
10.3060(3)	Zr, 4*a*	0	0	0	0.31(8)
	Cs, 8*c*	1/4	1/4	1/4	0.46(4)
	Cl, 24*e*	0.2321(4)	0	0	0.49(8)
Texture axis and parameter: [111] 0.132(3)					
	T = 300 K (R_I = 0.134, R_P = 0.461)				
10.4331(6)	Zr, 4*a*	0	0	0	1.4(2)
	Cs, 8*c*	1/4	1/4	1/4	0.79(8)
	Cl, 24*e*	0.2248(8)	0	0	0.5(2)
Texture axis and parameter: [111] 0.134(6)					

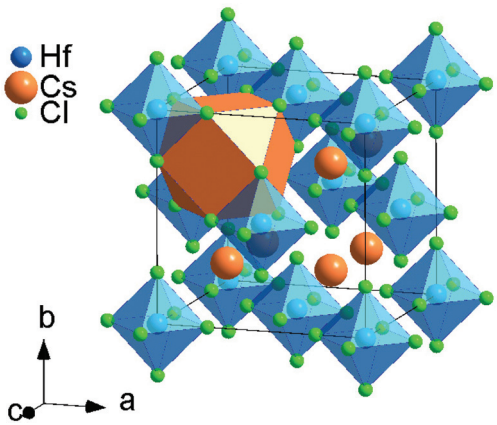

Fig. 4 Polyhedral view of the Cs_2HfCl_6 structure showing isolated [$HfCl_6$] octahedra and [$CsCl_{12}$] cubooctahedron.

Taking into account that members of this family may exhibit structural instability,[32] it was important to check for a possible phase transition at low temperatures. Our structural studies confirmed the same cubic structure (space group *Fm3m*) for Cs_2HfCl_6 and Cs_2ZrCl_6 over the whole examined temperature range.

Fig. 5 shows that cooling the samples causes only gradual decrease of the lattice constant due to thermal contraction of the crystals. No anomalies pointing to possible changes of the

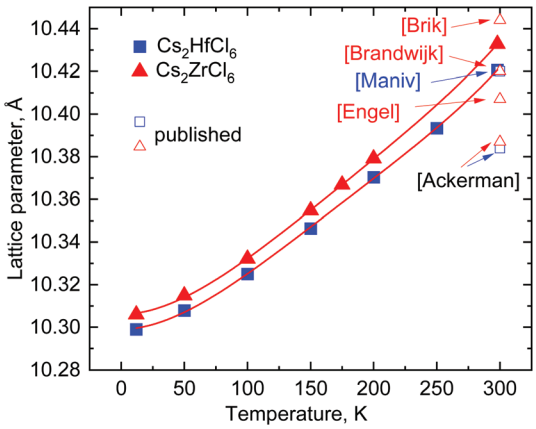

Fig. 5 The temperature dependence of the lattice parameters of Cs_2HfCl_6 and Cs_2ZrCl_6. For comparison the published values of the lattice parameters are shown as open blue squares (Cs_2HfCl_6) and open red triangles (Cs_2ZrCl_6) The red lines display fitting of the experimental data to the eqn (1).

crystal structure of these materials are observed in the low temperature range. The measured temperature dependencies of the lattice parameters are fitted using a nonlinear function:[33]

$$a(T) = a_0(1 + a_1T^2 + a_2T^3 + a_3T^4) \quad (1)$$

where a_0 is lattice size at T = 0 K, $a_1 \cdots a_3$ are fitting constants. The parameters of the fitting are given in Table 3.

3.2. Scintillation response at room temperature

To attest the scintillation performance of Cs_2HfCl_6 and Cs_2ZrCl_6 crystals we first measured their scintillation response at room temperature using a γ-ray source. The energy resolution (FWHM) and relative light yield were derived from the pulse height spectra of the crystals obtained at 662 keV γ-rays excitation from a ^{137}Cs source (Fig. 6). In addition to the well resolved 662 keV photopeak the spectra show the Compton continuum, a backscatter peak and a peak at 32 keV corresponding to X-rays from barium emitted during decay of ^{137}Cs. The obtained values of relative light yield and the energy resolution of the crystals are summarised in the Table 4. These results show that the relative light yield and energy resolution of Cs_2HfCl_6 crystal measured in this work is inferior in comparison with the published results. In contrast, Cs_2ZrCl_6 exhibits much higher light yield 33 900 ± 1700 ph per MeV than previously reported (25 100 ± 1200 ph per MeV (ref. 3)) and very encouraging energy resolution 4.5%. This finding demonstrates that Cs_2ZrCl_6 scintillator is well suited for

Table 3 Parameters of the fit for temperature dependence of lattice constants of Cs_2HfCl_6 and Cs_2ZrCl_6 crystals obtained using eqn (1)

Crystal	a_0, Å	$a_1 \times 10^{-7}$	$a_2 \times 10^{-9}$	$a_3 \times 10^{-12}$
Cs_2HfCl_6	10.2991(7)	3.76(21)	−1.44(16)	2.10(33)
Cs_2ZrCl_6	10.3061(5)	3.71(21)	−1.36(18)	1.95(37)

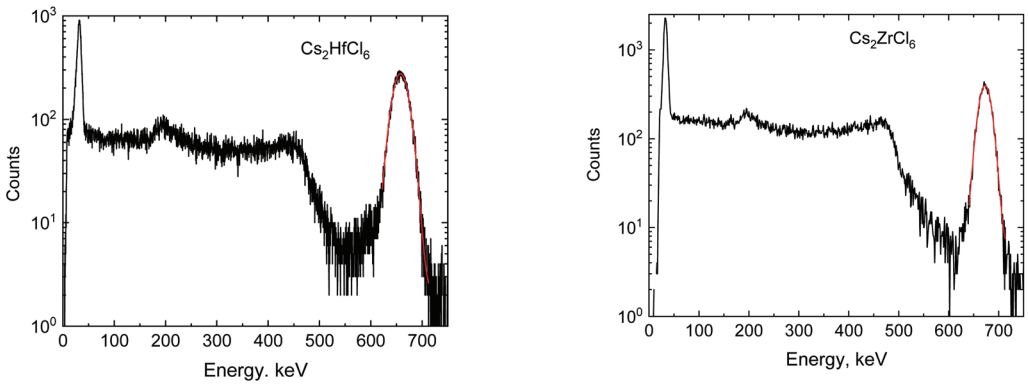

Fig. 6 Pulse height spectra of Cs_2HfCl_6 and Cs_2ZrCl_6 scintillators measured during excitation by 662 keV γ-rays of ^{137}Cs source (shaping time is equal to 10 μs). The red line shows the Gaussian fit of the photopeak.

Table 4 Scintillation characteristics of Cs_2HfCl_6 and Cs_2ZrCl_6 crystals at 9 and 295 K

	Light yield[a], ph per MeV		Light yield, ph per MeV	Energy resolution, %	Alpha-to-beta ratio	Scintillation pulse decay constants[b], μs						
						295 K			9 K			
Crystal	295 K	9 K	295 K	295 K	295 K	τ_1	τ_2	τ_3	τ_1	τ_2	τ_3	Ref.
Cs_2HfCl_6	19 600	25 700	24 800	5.3	0.39	0.4	5.1	15.2	0.6	12.0	76.0	This work
			54 000	3.3		0.3	4.4	n.d.				2
			30 000	3.3		0.4	3.9	n.d.				20
			36 400	4.1		0.9	4.4	n.d.				6
			26 800	4.3		1.0	5.0	12.0				16
			27 000	2.8		0.3	3.4	n.d.				8
Cs_2ZrCl_6	31 150	35 800	33 900	4.5	0.35	0.4	2.7	12.5	1.1	18.7	95.0	This work
			25 100	n.d.		1.5	7.5	n.d.				3

n.d. – not detected. [a] The relative light yield determined during excitation by 5.5 MeV alpha particles of ^{241}Am is converted to the light yield corresponding to gamma quanta based on alpha-to-beta ratios of the crystals. [b] Scintillation decay constants measured under irradiation by 5.5 MeV alpha particles of ^{241}Am.

γ-spectroscopy. The obtained alpha-to-beta ratio (or quenching factor) is similar for both crystals and close to that reported in the literature.[34]

It should be noted that the values presented in Table 4 were obtained with the shaping time equal to 10 μs. Increasing the shaping time from 0.5 to 10 μs results in a significant augmentation of the detected relative light yield: it quadrupled in Cs_2HfCl_6 and increased by factor of 7 in Cs_2ZrCl_6. This is due to the strong contribution of the slow decay components to the scintillation pulses constituting *ca.* 50% of the total intensity (see also discussion in sec. 3.3). The obtained results also evidence that the fractional contribution of this slow component is much stronger in Cs_2ZrCl_6.

3.3. Scintillation light output and decay time with temperature

To examine the behaviour of Cs_2MCl_6 crystal scintillators over a wide temperature range we measured the temperature dependence of the light output under α-particle excitation over 9–295 K. The crystals exhibit a very strong scintillation response manifested as clearly resolved peaks from α-particles of ^{241}Am. The pulse height spectra of the crystals at different temperatures are shown in Fig. 7.

The scintillation response of a reference material, $CaWO_4$ (provided by Institute of Single Crystals SRC "Carat" Lviv, Ukraine), and the measured values of alpha-to-beta ratio at room temperatures were used to derive the light yield of the crystals under study, in the same way as described in ref. 12. The scintillation light yields obtained for Cs_2HfCl_6 and Cs_2ZrCl_6 crystals under α-particle excitation are 19 600 ± 2900 photons per MeV and 31 150 ± 3700 photons per MeV, respectively (see Table 4). Both values are slightly less than that measured with the γ-source. This discrepancy could be due to the applied conversion procedure that assumes identical light collection from the reference and test crystals.[12] This assumption does not account for the difference in optical properties of materials (refraction, absorption, and scattering) affecting the light collection and leads to underestimation of the scintillation light yield.[35]

The measurements with varying temperature revealed unusual dependencies of scintillation light output in both crystals (Fig. 8). They are distinctly different to the gradual

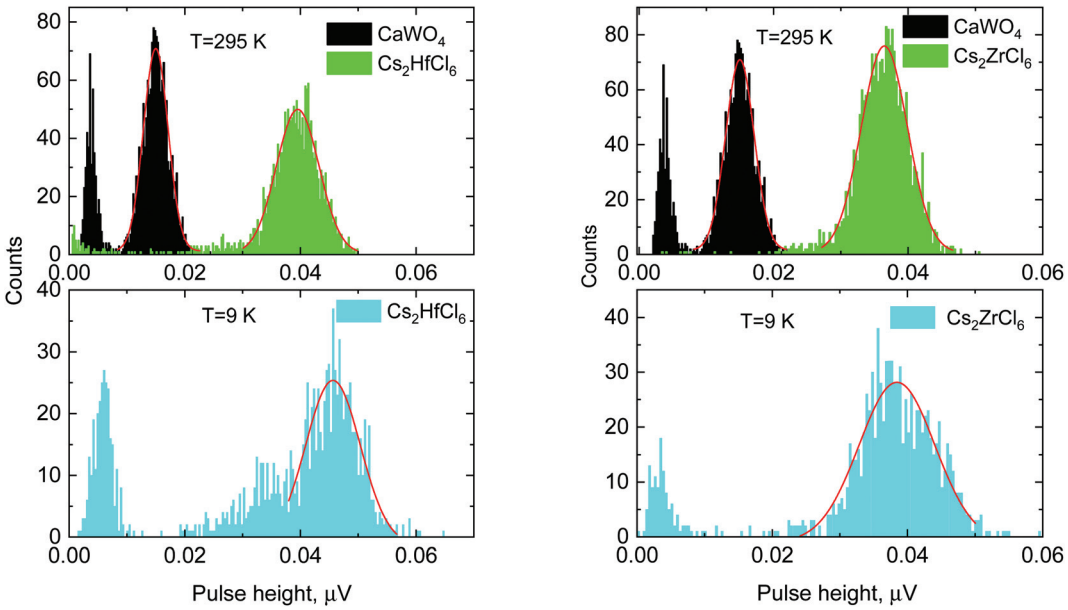

Fig. 7 Pulse height spectra of Cs_2HfCl_6 and Cs_2ZrCl_6 scintillators measured at 295 and 9 K during excitation by 5.5 MeV alpha particles of ^{241}Am. The red lines show the Gaussian peak fits.

decrease of scintillation light yield observed with increasing temperature in the majority of undoped scintillators.[36] The light output of Cs_2MCl_6 initially decreases with heating, but after reaching a minimum at *ca.* 100 K it increases. The trend changes again around 130 K after which the light output shows gradual decrease with temperature.

This feature is particularly evident in Cs_2ZrCl_6 crystals which exhibits *ca.* 50% increase of the light yield at T = 125 K in comparison with that at room temperature. It should be noted that this behavior of the emission intensity with temperature is very similar to that reported recently in ref. 10 and 12 where the decrease of the light yield observed below 100 K was attributed to the freeze-out of V_k-centers involved in the emission of self-trapped excitons (STE) in the crystals.

This type of temperature dependence termed as a "negative thermal quenching" has been observed before in some materials[37] including scintillators.[38,39] Assuming thermally activated crossover as the main mechanism that controls the population of involved states, this behavior can be explained by the thermal activation of intermediate trap states that leads to the enhancement of the emission intensity with increasing temperature. This can occur before the onset of non-radiative thermal quenching that causes a gradual decrease of emission intensity or during such quenching. In the presence of such processes, the model developed in ref. 37 gives the following expression for the temperature dependence of the emission intensity:

$$I(T) = I_0 \frac{1 + D_1 \exp\left(-\frac{E'_1}{kT}\right)}{1 + C_1 \exp\left(-\frac{E_1}{kT}\right) + C_2 \exp\left(-\frac{E_2}{kT}\right)}. \quad (2)$$

In eqn (2), I_0 is the total emission intensity at zero temperature, D_1, C_1 and C_2 are the transition rate constants, E'_1 is the

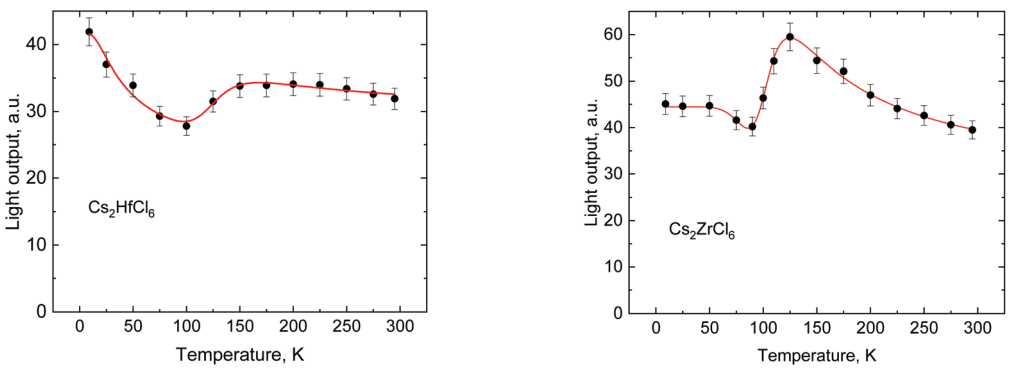

Fig. 8 Temperature dependence of the scintillation light output of Cs_2HfCl_6 and Cs_2ZrCl_6 measured under excitation by 5.5 MeV alpha particles from an ^{241}Am source. The red lines show fits of eqn (2) to the experimental results using parameters from Table 5.

activation energy necessary to promote the trapped particles to the emission state, E_1 and E_2 are the activation energies for the non-radiative quenching and k is the Boltzmann constant. Thus, the numerator is responsible for the emission enhancement due to the thermal release of particles from the intermediate traps to the emitting states. In turn, the denominator describes the processes of thermally activated non-radiative quenching of the emitting state.

Eqn (2) was used to fit the data in Fig. 8 demonstrating a good agreement between the experimental results and theoretical model. The parameters of the fit are summarised in Table 5. The attribution of intermediate levels to hole trapping centres has already been established in these materials.[10,12,17] The values of activation energy E'_1 (0.11 and 0.12 eV in Cs_2HfCl_6 and Cs_2ZrCl_6, respectively) correlate well with the activation energy of V_k-centres further supporting the earlier assumption that the carriers released in this process are the cause of increase of the light yield.

The parameters obtained from the analysis of temperature-dependent light yield reveal an interesting feature: in both crystals the energy required to promote the trapped particles to the emission state E'_1 is significantly larger than the first activation energy of thermal quenching E_1 while it is very close to the value of the second activation energy E_2. The observed features of temperature dependence of the light yield can be explained using the schematic configuration coordinate diagram in Fig. 9. In the proposed model, the non-radiative quenching due to crossover from the excited to the ground state that requires activation energy E_1 starts at low temperature (process 1). As the temperature increases, the thermal energy of the system reaches value E'_1 enabling promotion of the trapped particle to the emitting level (process 2) and enhancing the emission intensity. Further increase of temperature enables straight depletion of intermediate traps through the thermally activated two-step process – from traps to the excited state and then crossover to the ground state (process 3) – leading to the decrease of emission intensity. Fig. 9 also reveals that the energy E_2 needed to activate trap depletion should be equal to the sum $E'_1 + E_1$. It is worth noting that the values of the activation energies derived from the fitting to the model fulfil this condition within the uncertainties.

Fig. 10 shows the scintillation decay curves of Cs_2HfCl_6 and Cs_2ZrCl_6 crystals measured at different temperatures. The

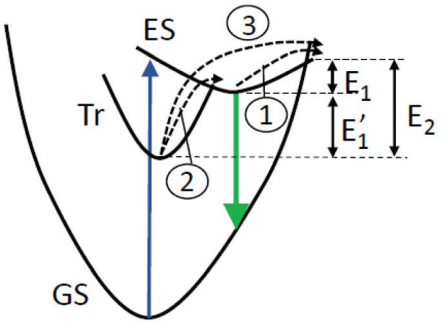

Fig. 9 Configuration coordinate diagram explaining the temperature dependence of luminescence in Cs_2HfCl_6 and Cs_2ZrCl_6. The vertical blue and green lines show excitation and emission transitions between ground state (GS) and exited state (ES) of the emission centre. The dotted lines represent the thermally-activated processes: 1- crossover from the excited to the ground state, 2- activation of traps (Tr) and 3- non-radiative decay of the traps *via* two-step activation and crossover to the ground state.

measured decay curves display a complex non-single exponential shape that is a characteristic feature of decay kinetics due to a superposition of a few recombination processes. The decay curves were fitted using three exponential functions that ensure the best quality of the fit in the entire range of temperatures. It should be noted though, that in the case of complex decay, such fits are merely a way of quantifying the measured decay curves and the fit parameters are not directly related to the specific emission processes occurring in the material.

The numerical values derived from the fit are presented in Fig. 11 and 12. Comparison of the parameters reveals a pronounced change of decay rate with temperature in Cs_2ZrCl_6. In Cs_2HfCl_6 only the slow decay time constant (τ_3) exhibits noticeable increase with cooling from room temperature to 200 K, while other decay time constants are mildly affected (see Fig. 11, left). The fractional content of amplitudes also changes insignificantly within *ca.* ± 10% with temperature (see Fig. 11, right). In contrast, for Cs_2ZrCl_6 all decay time constants and amplitudes experience tangible changes with cooling from room temperature as is demonstrated in Fig. 12.

An interesting feature is observed in Cs_2ZrCl_6 at 125 K. The decay time constants exhibit a prompt twofold rise followed by a quick drop. Since this feature correlates in temperature with the increase of the scintillation light output, we consider this observation as another manifestation of above-mentioned processes of the thermal activation of emission centers. Release of trapped charges at this temperature causes not only increase of the scintillation intensity but also slows down the emission. Once it is completed, the emission rate is accelerating again due to thermal quenching. This is accompanied by the changes in the fractional content of the fast and the slow decay components. Comprehensive modelling of intensity evolution with time and temperature in these materials is known to be a challenging task[10,11] that is beyond the scope of present study.

Table 5 Parameters of the fit obtained from the temperature dependence of the scintillation light output of Cs_2HfCl_6 and Cs_2ZrCl_6 crystals using eqn (2)

Parameter	Cs_2HfCl_6	Cs_2ZrCl_6
I_0	41.6(9)	44.4(6)
D_1	2.1×10^4	2.1×10^6
E'_1, eV	0.11(5)	0.12(8)
C_1	0.84	105
E_1, eV	0.005(1)	0.043(14)
C_2	3.1×10^4	3.3×10^6
E_2, eV	0.11(5)	0.13(7)

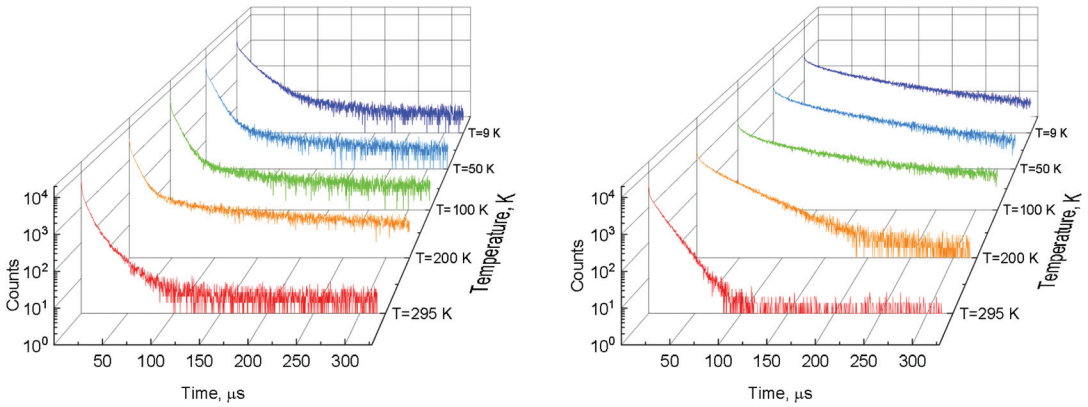

Fig. 10 Scintillation decay curves of Cs_2HfCl_6 (left) and Cs_2ZrCl_6 (right) crystals measured at different temperatures under excitation by 5.5 MeV alpha particles of an ^{241}Am source.

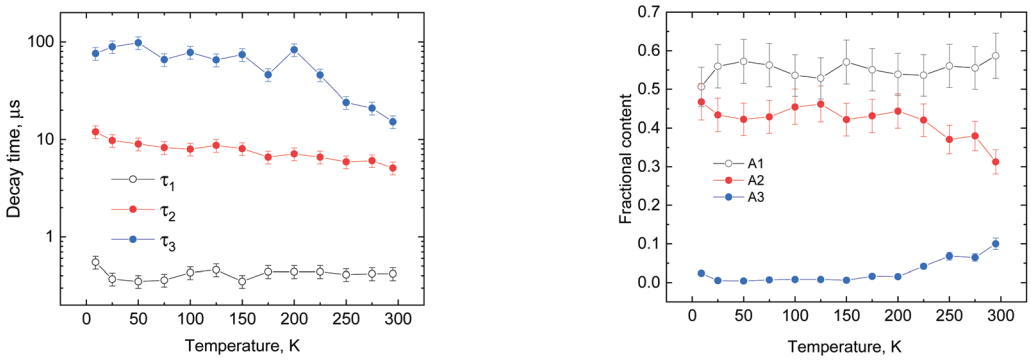

Fig. 11 Temperature dependence of decay time constants (left) and their amplitudes (right) obtained from the fitting of the decay curves of Cs_2HfCl_6, by a sum of three exponential functions.

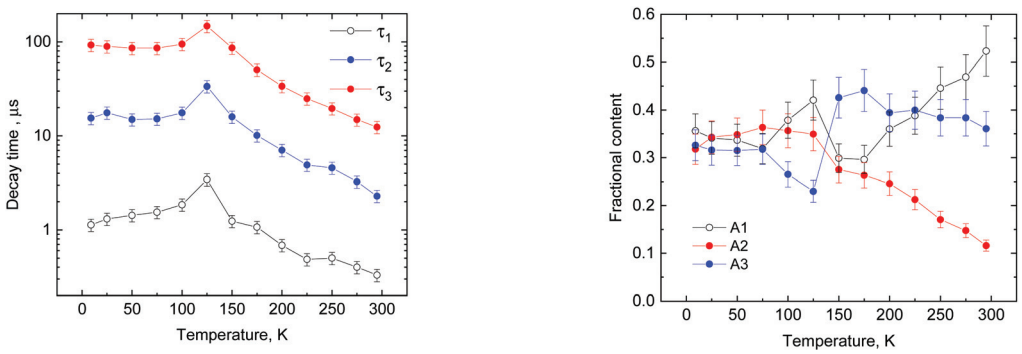

Fig. 12 Temperature dependence of decay time constants (left) and their amplitudes (right) obtained from the fitting of the decay curves of Cs_2ZrCl_6 by a sum of three exponential functions.

4. Conclusions

Metal hexachloride crystals Cs_2MCl_6 (M = Hf, Zr) belong to a new class of materials with promising scintillation characteristics. For scintillation applications, it is important to understand and control the quality and emission properties of the crystals. In this work we investigated the crystal structure and scintillation properties of Cs_2HfCl_6 and Cs_2ZrCl_6 over a wide (12–300 K) temperature range. XRD analysis revealed a gradual decrease of lattice parameters with cooling over this temperature range, ruling out the possibility of phase transition in the crystals. We measured the relative light yield, energy resolution and alpha-to-beta ratio of these scintillators at room temperature. The light yield of Cs_2HfCl_6 under excitation with a ^{137}Cs γ-source

is found to be 24 800 ± 1200 photons per MeV along with 5.3% energy resolution. Cs_2ZrCl_6 exhibits a higher light yield, 33 900 ± 1700 photons per MeV, resulting in an excellent energy resolution of 4.5%. The alpha-to-beta ratios determined with 5.5 MeV α-particles of an ^{241}Am source are equal to 0.39 ± 0.02 and 0.35 ± 0.02 for Cs_2HfCl_6 and Cs_2ZrCl_6 crystals, respectively.

The evolution of the scintillation light output and decay characteristics of the crystals with temperature was investigated under excitation with 5.5 MeV α-particles of ^{241}Am. We observed a significant enhancement of the light output in the 125–150 K temperature range that is attributed to a negative thermal quenching. The effect is explained as a thermal activation of the intermediate trap states that leads to the population of excited states. A consistent interpretation of the temperature changes in these crystals was achieved in a generalized phenomenological model. Using this model, we derived the numerical parameters that quantify the individual processes and constructed the energy scheme of the emission centre. The results of these studies provide better understanding of thermal changes in these crystalline materials. The results also motivate more in-depth study of the physical properties of these materials and underpin the strategy for development of scintillators with improved performance characteristics.

Conflicts of interest

The authors declare no conflict of interest.

Acknowledgements

L. V. acknowledges support of the National Research Foundation of Ukraine under grant no. 2020.02/0373 "Crystalline phosphors' engineering for biomedical applications, energy saving lighting and contactless thermometry". S. S. N., V. V. N. and P. W. are supported by the Arthur B. McDonald Canadian Astroparticle Physics Research Institute, with equipment funded by the Canada Foundation for Innovation and the Province of Ontario and housed at the Queen's Centre for Advanced Computing. Research at the Perimeter Institute is supported by the Government of Canada through the Department of Innovation, Science, and Economic Development, and by the Province of Ontario. We would like to thank Dr G. Stenning for XRD measurements on the Rigaku SmartLab diffractometer in the Materials Characterisation Laboratory at the ISIS Neutron and Muon Source.

References

1 C. Dujardin, E. Auffray, E. Bourret-Courchesne, P. Dorenbos, P. Lecoq, M. Nikl, A. N. Vasil'ev, A. Yoshikawa and R. Y. Zhu, Needs, Trends, and Advances in Inorganic Scintillators, *IEEE Trans. Nucl. Sci.*, 2018, **65**, 1977–1997.

2 A. Burger, E. Rowe, M. Groza, K. M. Figueroa, N. J. Cherepy, P. R. Beck, S. Hunter and S. A. Payne, Cesium hafnium chloride: A high light yield, non-hygroscopic cubic crystal scintillator for gamma spectroscopy, *Appl. Phys. Lett.*, 2015, **107**, 143505.

3 K. Saeki, Y. Fujimoto, M. Koshimizu, T. Yanagida and K. Asai, Comparative study of scintillation properties of Cs2HfCl6 and Cs2ZrCl6, *Appl. Phys. Express*, 2016, **9**, 042602.

4 C. Cardenas, A. Burger, M. L. DiVacri, B. Goodwin, M. Groza, M. Laubenstein, S. Nagorny, S. Nisi and E. Rowe, Internal contamination of the Cs2HfCl6 crystal scintillator, *Nucl. Instrum. Methods Phys. Res., Sect. A*, 2017, **872**, 23–27.

5 V. Caracciolo, S. S. Nagorny, P. Belli, R. Bernabei, F. Cappella, R. Cerulli, A. Incicchitti, M. Laubenstein, V. Merlo, S. Nisi and P. Wang, Search for alpha decay of naturally occurring Hf-nuclides using a Cs2HfCl6 scintillator, *Nucl. Phys. A*, 2020, **1002**, 121941.

6 C. Delzer, M. Zhuravleva, L. Stand, C. Melcher, N. Cherepy, S. Payne, R. Sanner and J. P. Hayward, Observations regarding inclusions in the growth of Cs2HfCl6 single crystal scintillators, *J. Cryst. Growth*, 2020, **531**, 125336.

7 R. Hawrami, E. Ariesanti, V. Buliga, S. Motakef and A. Burger, Latest Progress on Advanced Bridgman Method-Grown K2PtCl6 Cubic Structure Scintillator Crystals, *IEEE Trans. Nucl. Sci.*, 2020, **67**, 1020–1026.

8 E. Ariesanti, R. Hawrami, A. Burger and S. Motakef, Improved growth and scintillation properties of intrinsic, non-hygroscopic scintillator Cs2HfCl6, *J. Lumin.*, 2020, **217**, 116784.

9 B. Kang and K. Biswas, Carrier Self-trapping and Luminescence in Intrinsically Activated Scintillator: Cesium Hafnium Chloride (Cs2HfCl6), *J. Phys. Chem. C*, 2016, **120**, 12187–12195.

10 R. Kral, V. Babin, E. Mihokova, M. Buryi, V. V. Laguta, K. Nitsch and M. Nikl, Luminescence and Charge Trapping in Cs2HfCl6 Single Crystals: Optical and Magnetic Resonance Spectroscopy Study, *J. Phys. Chem. C*, 2017, **121**, 12375–12382.

11 M. Koshimizu, K. Saeki, Y. Fujimoto, G. Okada, T. Yanagida, S. Yamashita and K. Asai, A three-state model for describing the temperature variation of the scintillation properties of Cs2HfCl6, *Jpn. J. Appl. Phys.*, 2018, **57**, 032401.

12 M. Buryi, V. Babin, R. A. M. Ligthart, S. S. Nagorny, V. B. Mikhailik, V. Vaněček, L. P. Prochazková, R. Kandel, V. V. Nahorna and P. Wang, Correlation of emission, scintillation and charge trapping properties in Cs_2HfCl_6 and Cs_2ZrCl_6 single crystals, *J. Mater. Chem. C*, 2021, **9**, 2955–2968.

13 K. Saeki, Y. Fujimoto, M. Koshimizu, D. Nakauchi, H. Tanaka, T. Yanagida and K. Asai, Luminescence and scintillation properties of Tl- and Ce-doped Cs2HfCl6 crystals, *Jpn. J. Appl. Phys.*, 2017, **56**, 020307.

14 Y. Fujimoto, K. Saeki, D. Nakauchi, H. Fukada, T. Yanagida, H. Kawamoto, M. Koshimizu and K. Asai, Photoluminescence, photoacoustic, and scintillation properties of Te4+-doped Cs2HfCl6 crystals, *Mater. Res. Bull.*, 2018, **105**, 291–295.

15 S. Kodama, S. Kurosawa, J. Pejchal, R. Kral, A. Yamaji, Y. Ohashi, Y. Yokota, K. Kamada, M. Nikl and A. Yoshikawa, Growth and Luminescent Properties of

Cs2HfCl6 Scintillators Doped With Alkaline Earth Metals, *IEEE Trans. Nucl. Sci.*, 2018, **65**, 2169–2173.
16 V. Vanecek, J. Paterek, R. Kral, M. Buryi, V. Babin, K. Zlouzeova, S. Kodama, S. Kurosawa, Y. Yokota, A. Yoshikawa and M. Nikl, Cs2HfCl6 doped with Zr: Influence of tetravalent substitution on scintillation properties, *J. Cryst. Growth*, 2021, **573**, 126307.
17 M. Buryi, R. Kral, V. Babin, J. Paterek, V. Vanecek, P. Veverka, M. Kohoutkova, V. Laguta, M. Fasoli, I. Villa, F. Cova, A. Vedda and M. Nikl, Trapping and Recombination Centers in Cesium Hafnium Chloride Single Crystals: EPR and TSL Study, *J. Phys. Chem. C*, 2019, **123**, 19402–19411.
18 K. Saeki, Y. Wakai, Y. Fujimoto, M. Koshimizu, T. Yanagida, D. Nakauchi and K. Asai, Luminescence and scintillation properties of Rb2HfCl6 crystals, *Jpn. J. Appl. Phys.*, 2016, **55**, 110311.
19 K. Saeki, Y. Fujimoto, M. Koshimizu, D. Nakauchi, H. Tanaka, T. Yanagida and K. Asai, Luminescence and scintillation properties of Cs2HfBr6 and Cs2ZrBr6 crystals, *Jpn. J. Appl. Phys.*, 2018, **57**, 030310.
20 S. Lam, C. Guguschev, A. Burger, M. Hackett and S. Motakef, Crystal growth and scintillation performance of Cs2HfCl6 and Cs2HfCl4Br2, *J. Cryst. Growth*, 2018, **483**, 121–124.
21 P. Bhattacharya, C. Brown, C. Sosa, M. Wart, S. Miller, C. Brecher and V. V. Nagarkar, Tl2ZrCl6 and Tl2HfCl6 Intrinsic Scintillators for Gamma Rays and Fast Neutron Detection, *IEEE Trans. Nucl. Sci.*, 2020, **67**, 1032–1034.
22 R. Hawrami, E. Ariesanti, V. Buliga, L. Matei, S. Motakef and A. Burger, Advanced high-performance large diameter Cs2HfCl6 (CHC) and mixed halides scintillator, *J. Cryst. Growth*, 2020, **533**, 125473.
23 S. Nagorny, Novel Cs2HfCl6 Crystal Scintillator: Recent Progress and Perspectives, *Physics*, 2021, **3**, 320–351.
24 S. Maniv, Crystal Data for Cs2HfCl6, *J. Appl. Crystallogr.*, 1976, **9**, 245–245.
25 J. F. Ackerman, Preparation and Luminescence of Some [K2PtCl6] Materials, *Mater. Res. Bull.*, 1984, **19**, 783–791.
26 L. Akselrud and Y. Grin, WinCSD: software package for crystallographic calculations (Version 4), *J. Appl. Crystallogr.*, 2014, **47**, 803–805.
27 V. B. Mikhailik and H. Kraus, Development of techniques for characterisation of scintillation materials for cryogenic application, *Radiat. Meas.*, 2013, **49**, 7–12.
28 G. Engel, Die Kristallstrukturen einiger Hexachlorokomplexsalze, *Z. Kristallogr.*, 1935, **90**, 341–373.
29 R. Liu, W. Zhang, G. Li and W. Liu, An ultraviolet excitation anti-counterfeiting material of Sb3+ doped Cs2ZrCl6 vacancy-ordered double perovskite, *Inorg. Chem. Front.*, 2021, **8**, 4035–4043.
30 V. Brandwijk and D. L. Jongejan, The effect of pressure on A2BX6 halides, contrary to the effect of pressure on ABX3 halides, *Mater. Res. Bull.*, 1972, **7**, 635–639.
31 M. G. Brik and I. V. Kityk, Modeling of lattice constant and their relations with ionic radii and electronegativity of constituting ions of AXY cubic crystals (A=K, Cs, Rb, Tl; X=tetravalent cation, Y=F, Cl, Br, I), *J. Phys. Chem. Solids*, 2011, **72**, 1256.
32 D. I. Torres, J. D. Freire and R. S. Katiyar, Lattice dynamics of crystals having R2MX6 structure, *Phys. Rev. B: Condens. Matter Mater. Phys.*, 1997, **56**, 7763–7766.
33 A. Senyshyn, H. Kraus, V. B. Mikhailik and V. Yakovyna, Lattice dynamics and thermal properties of CaWO4, *Phys. Rev. B: Condens. Matter Mater. Phys.*, 2004, **70**, 214306.
34 C. Cardenas, A. Burger, B. Goodwin, M. Groza, M. Laubenstein, S. Nagorny and E. Rowe, Pulse-shape discrimination with Cs2HfCl6 crystal scintillator, *Nucl. Instrum. Methods Phys. Res., Sect. A*, 2017, **869**, 63–67.
35 V. Alenkov, O. A. Buzanov, N. Khanbekov, V. N. Kornoukhov, H. Kraus, V. B. Mikhailik and V. A. Shuvaeva, Application of the Monte-Carlo refractive index matching (MCRIM) technique to the determination of the absolute light yield of a calcium molybdate scintillator, *J. Instrum.*, 2013, **8**, P06002.
36 V. B. Mikhailik and H. Kraus, Scintillators for cryogenic applications: State-of-art, *J. Phys. Stud.*, 2010, **14**, 4201.
37 H. Shibata, Negative thermal quenching curves in photoluminescence of solids, *Jpn. J. Appl. Phys.*, 1998, **37**, 550–553.
38 S. Lam, M. Gascon, R. Hawrami, W. Setyawan, S. Curtarolo, R. S. Feigelson and R. M. Gaume, Nonproportionality and Scintillation Studies of Eu:SrI2 From 295 to 5 K, *IEEE Trans. Nucl. Sci.*, 2012, **59**, 2052–2056.
39 L. Swiderski, K. Brylew, W. Drozdowski, M. Grodzicka-Kobylka, L. Janiak and M. Moszynski, LuAG:Pr, LuAG:Pr, Mo and LuYAG:Pr relative light yield measured at wide temperature range with MPPC readout, *Nucl. Instrum. Methods Phys. Res., Sect. A*, 2022, **1021**, 165924.